

RESEARCH

Open Access



Comparisons Between Pull-Out Behaviour of Various Hooked-End Fibres in Normal–High Strength Concretes

Sadoon Abdallah* and David W. A. Rees

Abstract

In this paper an elastic–plastic response has been developed to predict the pull-out behaviour of various hooked end fibres embedded in normal–high strength concretes. An elastic–plastic moment expression has been proposed to represent the partially plastic hinge formed during pull-out. The proposed formula has been incorporated into a frictional pulley force analysis in order to predict the applied loading at each stage of pull-out. This prediction accounts for the variation of geometrical and tensile properties of the fibres as well as concrete strength. The proposed model is validated against experimental pull-out results of various hooked end fibres.

Keywords: pull-out behaviour, normal-high strength concrete, hooked end fibres, an elastic–plastic response, frictional pulley analysis

1 Introduction

The use of steel fibre reinforced concrete (SFRC) as an alternative to traditional rebar or mesh reinforcement has highly influenced the design of modern structures. Plain concrete is characterised by its brittle behaviour in tension (Zendaoui et al. 2016; Abdallah et al. 2018a, b). Steel fibres incorporated are dispersed within the concrete in order to improve its ductility, tensile behaviour and impact resistance (Tadepalli et al. 2013; Adjrad et al. 2016; Abdallah et al. 2018a, b). Of these the greatest advantage of including steel fibres in the concrete is to impart ductility to an otherwise brittle material. Steel fibres enable the concrete to continue carry load after cracking, the so-called post-cracking behaviour (Abdallah et al. 2016b; El-Mal et al. 2015). A further benefit of the addition of steel fibres is to impart extremely good crack resistance. High strength steel fibres when distributed homogeneously throughout the concrete matrix provide very effective crack control as there will always

be a fibre in the neighbourhood of a micro-crack, preventing the crack from growing.

The post-cracking behaviour of SFRC is closely related to the bond characteristics between the fibre and the matrix (Won et al. 2013; Abdallah et al. 2017c, d). The efficiency of fibres in bridging cracks depends upon the bond mechanisms associated with the pull-out behaviour (Islam and Alam 2013; Li and Liu 2016; Abdallah et al. 2017b). Tensile stress in the concrete matrix is transferred to the fibre through a characteristic durable bond at their interface. In order to increase the load-carrying capacity of SFRC, steel fibres with a variety of different shape and size are introduced. Hooked ends, enlarged ends, spiral, twisted and crimped are among the different designs available. Of these, Dramix hooked end fibres of 4D (double bend) and 5D (triple bend) geometries were developed specifically to increase the crack-bridging ability of SFRC. The high mechanical anchorage effect of these fibres was demonstrated in a number of prior studies showing that their strong bonding to the matrix resulted in a high resistance to pull-out (Abdallah and Fan 2017). Fibre with more a complex pre-deformed geometry place a higher complexity on the analysis of its pull-out response (Abdallah et al. 2017c, d). As the number of hook bends increases, both the maximum

*Correspondence: sadoon.abdallah@brunel.ac.uk
College of Engineering, Design and Physical Sciences, Brunel University
London, Uxbridge, London UB8 3PH, UK
Journal information: ISSN 1976-0485 / eISSN 2234-1315

pull-out load and pull-out work increase significantly. Numerous experimental investigations on the pull-out behaviour of pre-deformed fibres have been carried out to clarify the influence of fibre geometry on the bond-slip response (Isla et al. 2015; Tuyan and Yazici 2012; Soetens et al. 2013b; Robins et al. 2002). It has been shown from the pull-out test that a hooked end fibre is an effective method for improving the bond-slip resistance (Abdallah et al. 2017a).

Over the past four decades several analytical models have been proposed to predict the pull-out behaviour of steel fibres with various shapes (Lee et al. 2010; Nammur and Naaman 1989; Soetens et al. 2013a; Georgiadi-Stefanidi et al. 2010; Naaman et al. 1991a, b; Deng et al. 2018). The first attempts to predict the pull-out behaviour of hooked end fibres were advanced by (Chanvillard 1999) and (Alwan et al. 1999). Chanvillard model's is based on the concept of virtual work dividing the hook into distinct straight and curved parts. Alwan et al. (1999) used the frictional pulley analogue to determine the anchoring forces provided by the fibre hook. The latter's contribution is considered a function of the work needed to straighten the fibre during pull-out. Sujivorakul et al. (2000) extended the straight fibre pull-out analysis developed by Naaman et al. (1991a) by adding a non-linear spring to the end of the fibre to simulate the mechanical anchorage contribution.

In recent work, (Laranjeira et al. 2010; Lee et al. 2010; Ghoddousi et al. 2010) proposed alternatives to the pulley model of Alwan et al. (1999). Zile et al. (2013) developed an analytical model to simulate the mechanical contribution from fibre geometry to the pull-out response of crimped and hooked-end steel fibres. Their model is based both on the amount of plastic work required to straighten the fibre during pull-out and frictional resistance in the curved ducts. Won et al. (2015) extended this to the work required in straightening arch-type steel fibres.

The mechanics as explained in these theories involves a large number of parameters which are mostly restricted to a set of experimental boundary conditions and material properties. The rising applications of 4D and 5D hooked end fibres in modern structural applications have created the need to simplify theoretical analyses. For example, a semi-empirical pull-out analysis of these fibres was proposed by the authors to match observed behaviour satisfactorily (Abdallah et al. 2016a). This model adopted Alwan's frictional pulley (Alwan et al. 1999) to account for variations in mechanical and geometrical properties of the fibres as well as the matrix strength. Previously the authors (Abdallah et al. 2016a) examined fibre-matrix conditions for a pull-out force where a full straightening of the fibre was observed. This paper investigates the

conditions when the hook is not fully straightened during the pull-out as has been often observed. The elastic-plastic moment expression was advanced to represent the actual the plastic penetrations involved in the unbending required. Here again when taken with the frictional pulley concept (Abdallah et al. 2016a) this paper shows how plasticity explains the pull-out behaviour of 3D, 4D and 5D fibres embedded in a specific concrete matrix. It is shown how this approach is applied to experimental results for each hooked end fibre and three concrete matrices in normal-high strength range.

2 Experimental Program

2.1 Materials and Specimen

Three types of commercially available Dramix hooked end steel fibres, namely: 3DH (single bend), 4DH (double bend) and 5DH (triple bend) fibres were used in this study. These fibres have exactly the same length (60 mm), diameter (0.90 mm) and aspect ratio ($l_f/d_f=65$) but differ in their hook geometry and tensile strength. The measured geometrical and mechanical properties of these fibres (stacked) are depicted in Fig. 1 and detailed in Table 1. The average stress-strain curves of each fibre is shown in Fig. 2. To investigate the mechanical anchoring effect provided by each fibre hook, straight fibres (3DS, 4DS and 5DS) were obtained from the same hooked end fibres (3DH, 4DH and 5DH) by removing their hook ends.

Pull-out specimens were produced in three different concrete strengths, namely normal (NSC), medium (MSC) and high (HSC). Table 2 summarizes the materials used and mix proportions for all mixtures. Cubic specimens with a side dimension of 100 mm were used for single pull-out tests. Each cube contained three fibres embedded carefully to a depth of a half fibre length i.e. 30 mm. For each mix, five cubic specimens were also prepared for compressive strength tests. During casting, the dry materials (cement, silica fume, sand and crushed granite) were firstly mixed for approximately 1 min before water and superplasticizer (for the HSC) were added. This was then mixed for roughly 11 min. After casting and vibrating, the specimens were covered with a plastic sheet to avoid moisture loss and left for 24 h at room temperature. After that, they were demoulded and left to cure for a further 28 days in a conditioning chamber at 20 ± 2 °C and $96 \pm 4\%$ RH.

2.2 Test Setup

The pull-out tests were performed using a specially designed grip system, as illustrated in Fig. 3, which was attached to an Instron 5584 universal testing machine. The grips were designed such that the forces applied to the fibre would represent that in a fibre bridging a crack.

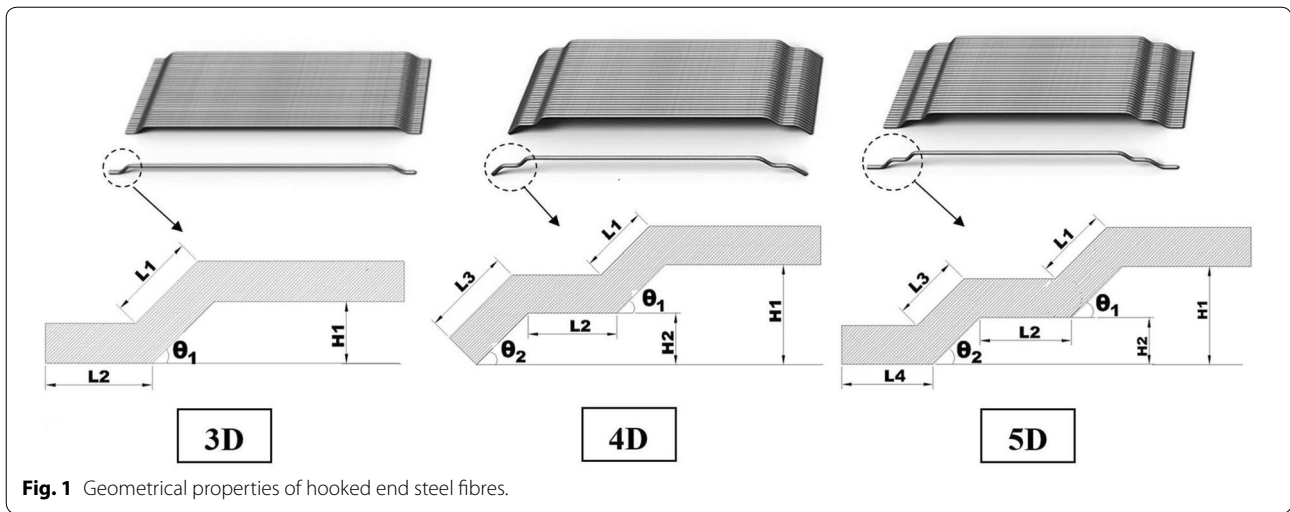


Fig. 1 Geometrical properties of hooked end steel fibres.

Table 1 The measured geometric and mechanical properties of hooked-end fibres.

Fibre type	σ_u^a (MPa)	σ_y^b (MPa)	l_f (mm)	d_f (mm)	Hook length (mm)				Hook angles (°)			Hook height (mm)	
					L1	L2	L3	L4	θ_1	θ_2	β	H1	H2
3D 65/60 BG	1150	775–985	60	0.90	2.12	2.95	–	–	45.7	45.5	67.5	1.85	–
4D 65/60 BG	1500	1020–1165	60	0.90	2.98	2.62	3.05	–	30.1	30.8	75.0	4.37	2.20
5D 65/60 BG	2300	1177–1455	60	0.90	2.57	2.38	2.57	2.56	27.9	28.2	76.0	2.96	1.57

^a Ultimate strength.

^b Yield strength.

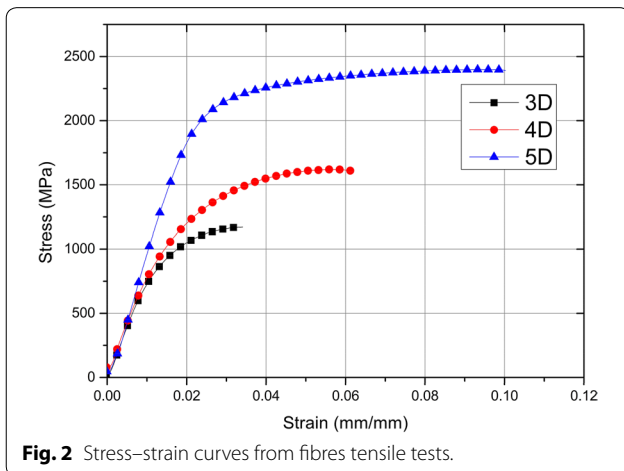


Fig. 2 Stress–strain curves from fibres tensile tests.

The body of the gripping system was machined in a lathe using mild steel and had a tapered end to allow the insertion of four M4 grub screws (Fig. 3). These were then tightened around the steel fibre to an equal torque for an even distribution of gripping pressure to minimise the deformation of the fibre ends and avoid breakage at the tip. Two linear variable differential transformer (LVDT)

transducers were used to measure the distance travelled by the steel fibre relative to the concrete face during testing (i.e. the pull-out distance). They were held in place using aluminium sleeves on either side of the main grip body (Fig. 3). The LVDT probes had ball bearings at their tips for accuracy in measurements taken from the top datum face. The sample was secured to the Instron base using clamps with riser blocks and M16 studs. The base rested on a round brass disc to retain flatness under test at a displacement rate of 10 μ m/s.

2.3 Experimental Results

The average pull-out-slip curves of (3DS, 4DS and 5DS) straight fibres pulled-out from a NSC, MSC and HSC is shown in Fig. 4a–c. These show that the pull-out behaviour of all straight behaviour is characterized by a rapid increase up to the peak load, followed by a sudden drop in the pull-out load, indicating full debonding of fibre/matrix interface. After that, the pull-out behaviour is controlled entirely by dynamic frictional resistance, where pull-out load gradually decreases with the increase in slip. For the same concrete grade, the maximum pull-out load (P_{max}) of 3DS, 4DS and 5DS fibres was quite similar, as expected. This is mainly due to the fact that straight

Table 2 Mix design of mixtures.

Concrete type	Mix proportions (kg/m ³)						W/B (-)	Compressive strength (MPa)
	Cement (type)	Fly ash	Aggregates	Sand	Superplasticizer	Water		
NSC	364 (32.5R)	–	979	812	–	200	0.55	33
MSC	350 (52.5N)	107	660	1073	–	205	0.45	54
HSC	480 (52.5N)	45	850	886	6	210	0.40	72

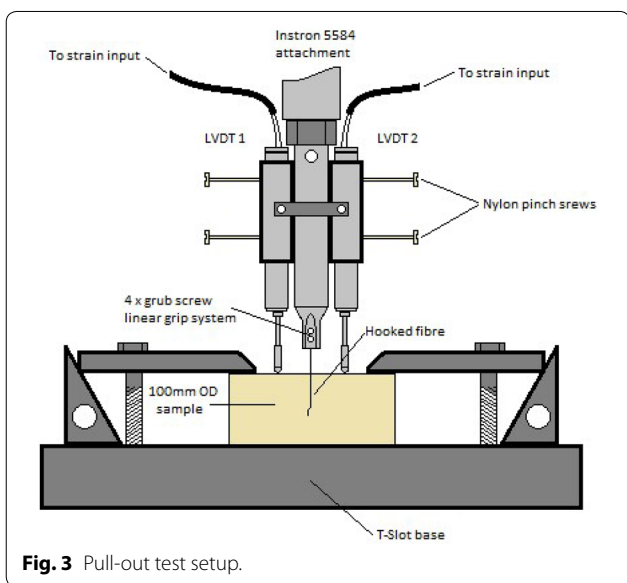


Fig. 3 Pull-out test setup.

fibres (without hooks) have the same geometry, diameter, and embedded length and hence the pull-out behaviour would remain almost the same. On the other hand, Fig. 4a–c show that P_{max} for all straight fibres increases significantly as the compressive strength of the concrete increase. Compared to the NSC, the percent increase in the P_{max} in the case of MSC and HSC is 40% and 98%, respectively as shown in Fig. 5.

The experimental pull-out-slip curves of (3DH, 4DH and 5DH) hooked end fibres pulled-out from a NSC, MSC and HSC matrix are presented in Figs. 6, 7 and 8. It can be seen that the initial pull-out response of hooked end fibres is again governed by a combination of two different mechanisms: debonding of the fibre–matrix interface and frictional slip of the fibre. However, in addition to these ‘straight-fibre’ mechanisms, mechanical interlock is introduced by the plastic deformation of the fibre hook. In contrast to a straight fibre, the mechanical anchorage contribution provided by a hooked end fibre increases the pull-out load after de-bonding significantly. It can be observed that P_{max} for all hook end fibres increases with an increase in matrix strength. It is also evident that an

increase in number of hook bends increases P_{max} dramatically. The 5DH (triple bend) fibres showed considerably higher values of P_{max} in all concrete matrices (Fig. 9). In addition, the pull-out work of 5DH fibre was significantly higher than that of the 3DH (single bend) and 4DH fibres (double bend). The higher performance for 5DH fibre is due to the high energy needed to deform and straighten the hook bends. However, despite the increased energy consumed during the pull-out, the full straightening of 4DH and 5DH hook bends was not observed (Fig. 10). However, the straightening of the hook increases significantly as the matrix strength increases e.g. a hooked end fibre pulled-out from the HSC showed higher levels of hook straightening that those of the NSC and MSC (Fig. 10). This indicates consistently that concrete matrix with higher strength is needed to ensure the hook bends are almost completely straightened. The benefit of this feature of fibre reinforcement is worth evaluating in the following section.

3 Elastic–Plastic Moment Expression

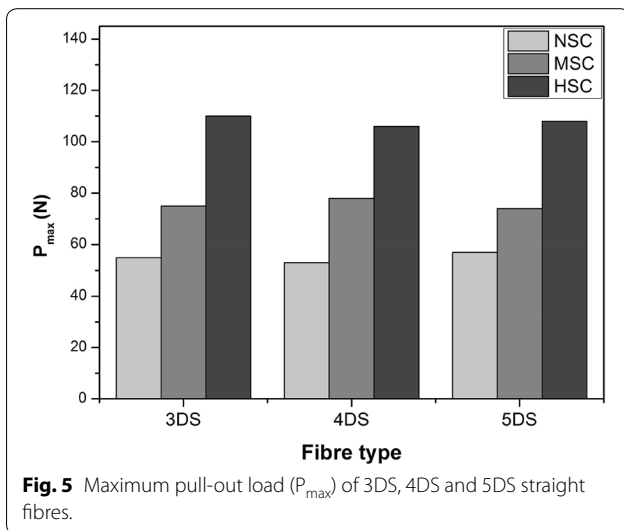
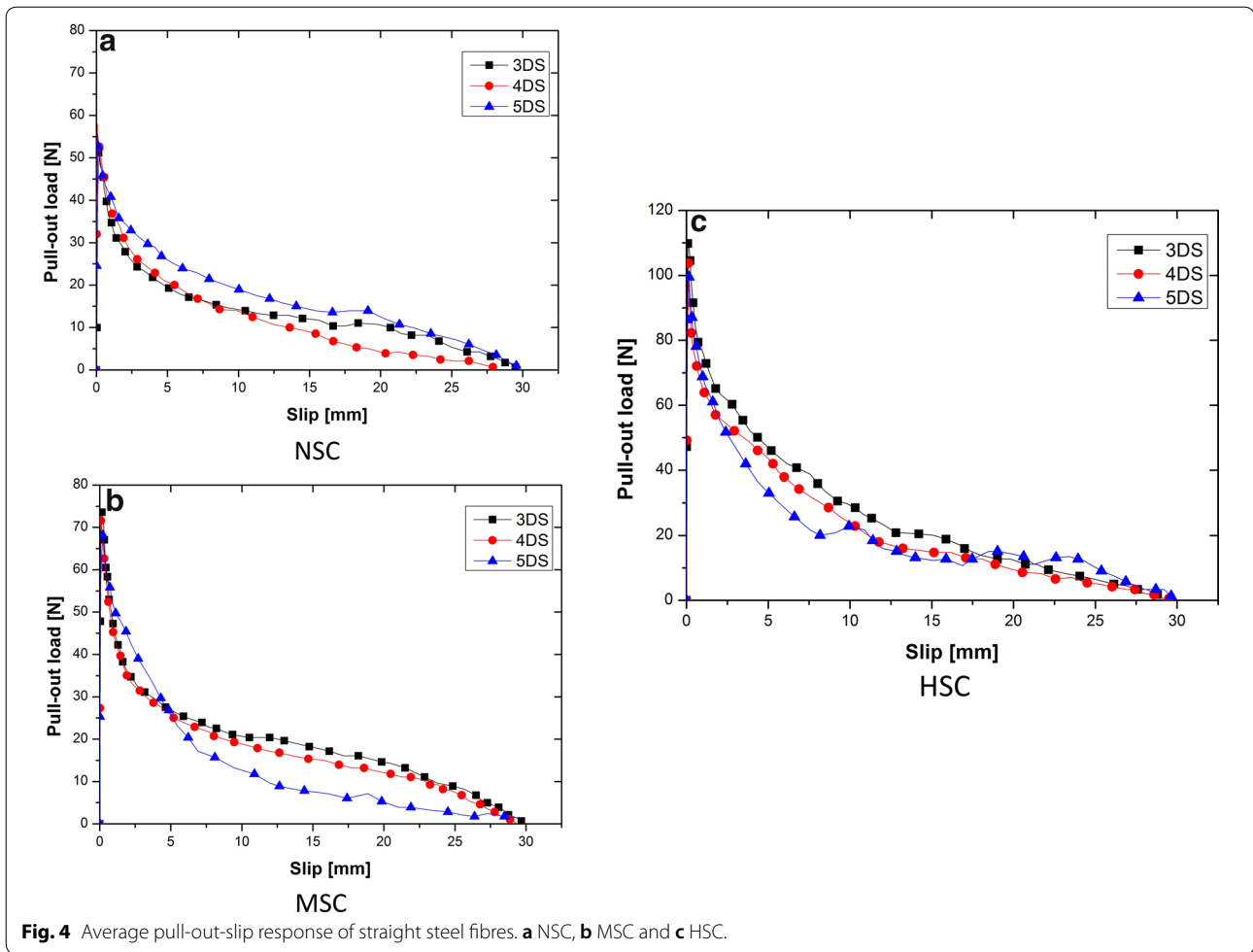
An estimate of the spread of plasticity within the hook bends is a necessary requirement when predicting the force required to pull-out an embedded fibre from a concrete matrix. What follows is based upon a wire bend of uniform curvature ‘equivalent’ to the various hook geometries i.e. 3D, 4DH and 5D fibres.

Consider a circular wire fibre section of radius r_f subjected to a uniform hogging bending moment M as shown in Fig. 11. A fully elastic moment M_E refers to that stress distribution given in which the yield stress σ_y has been reached at the top and bottom positions for the section in tension and compression respectively.

The moment M_E refers to a limiting condition at which the elastic theory of bending applies:

$$\frac{M_E}{I} = \frac{E_f}{\rho_E} = \frac{\sigma_y}{r_f} \tag{1}$$

in which E_f is the fibre modulus, ρ_E is the fully elastic curvature of the unstressed neutral axis (N.A) and $I = \int_A y^2 dA$ is the second moment of the section’s area



about the x-axis. The following relationships apply from re-arranging Eq. (1) when $I = \frac{\pi r_f^4}{4}$ for the fibre's circular section:

$$M_E = \frac{E_f I}{\rho_E} = \frac{\sigma_y I}{r_f} \tag{2}$$

$$\rho_E = \frac{E_f I}{M_E} = \frac{E_f r_f}{\sigma_y} \tag{3}$$

$$\therefore M_E = \frac{\pi E_f r_f^4}{4 \rho_E} = \frac{\pi \sigma_y r_f^3}{4} \tag{4}$$

When $M > M_E$ plastic zones penetrate inwards from the top and bottom to depth h as shown in Fig. 12. The new beam curvature ρ_e (Fig. 11) applies to the inner region of elastic material with reduced second moment of area I_e . The elastic-plastic moment M_{ep} is split with two contributions:

$$M_{ep} = M_e + M_p \tag{5}$$

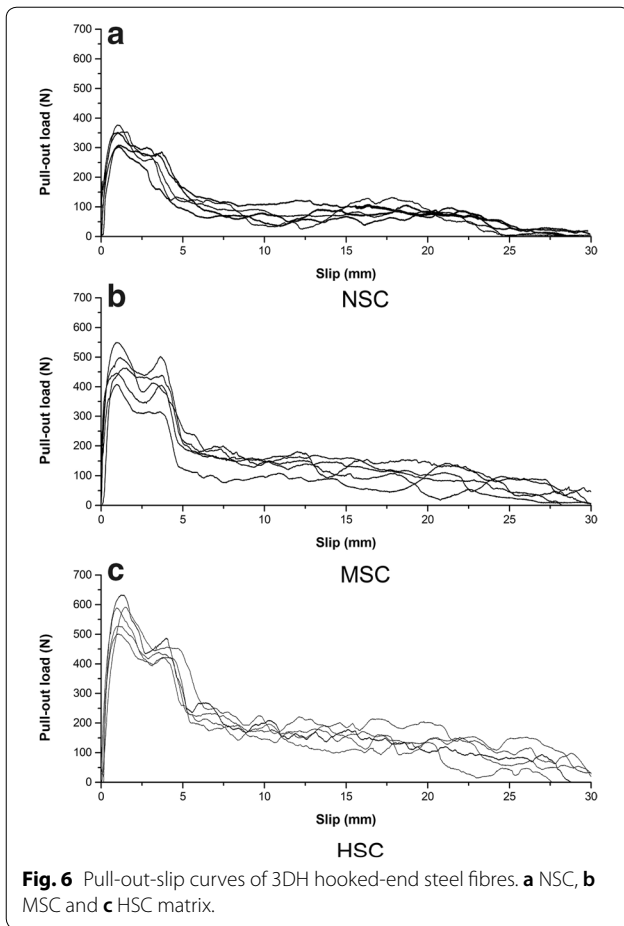


Fig. 6 Pull-out-slip curves of 3DH hooked-end steel fibres. **a** NSC, **b** MSC and **c** HSC matrix.

where the elastic contribution, M_e applies bending theory to an elastic core. Given the small diameter of wire this core is assumed to be circular of radius $r_f - h$ with a simplified second moment of area $I_e = \frac{\pi(r_f - h)^4}{4}$. Here, M_e and the elastic curvature ρ_e are given as:

$$M_e = \frac{\sigma_y I_e}{r_f - h} = \frac{\sigma_y \times \pi(r_f - h)^4}{4(r_f - h)} = \frac{\pi \sigma_y}{4} (r_f - h)^3$$

$$\rho_e = \frac{E_f(r_f - h)}{\sigma_y} = \frac{E_f r_f \left(1 - \frac{h}{r_f}\right)}{\sigma_y} \tag{6}$$

The plastic contribution M_p assumes that σ_y is uniformly distributed within each penetration area. For the strip area δA shown in the first diagram of Fig. 11, δM_p becomes the couple produced from the opposing parallel forces $\sigma_y \delta A$ separated by $2y$:

$$\delta M_p = 2\sigma_y \delta A y = 2\sigma_y \left[2(r_f^2 - y^2)^{1/2} \delta y\right] \times y$$

where δA is the bracketed quantity. Integrating between the limits of y as:

$$M_p = 4\sigma_y \int_{(r_f - h)}^{r_f} y(r_f^2 - y^2)^{1/2} dy$$

$$= -\frac{4}{2}\sigma_y \int_{(r_f - h)}^{r_f} -2y(r_f^2 - y^2)^{1/2} dy$$

$$M_p = \frac{4}{3}\sigma_y [h(2r_f - h)]^{3/2} \tag{7}$$

The sum of Eqs. (6) and (7) provides the elastic-plastic moment required for plastic penetration of each zone to depth h :

$$\therefore M_{ep} = \frac{\pi \sigma_y}{4} (r_f - h)^3 + \frac{4\sigma_y}{3} [h(2r_f - h)]^{3/2}$$

$$\times \begin{cases} \text{first yield } h = 0, M_E = \frac{\pi \sigma_y r_f^3}{4} \\ \text{fully plastic } h = r_f, M_P = \frac{4\sigma_y r_f^3}{3} \end{cases} \tag{8}$$

When Eq. (8) is normalised with the fully elastic moment in Eq. (1) it becomes:

$$\frac{M_{ep}}{M_E} = \frac{(r_f - h)^3}{r_f^3} + \frac{16}{3\pi r_f^3} [h(2r_f - h)]^{3/2}$$

which is written in a convenient dimensionless form:

$$\frac{M_{ep}}{M_E} = \left(1 - \frac{h}{r_f}\right)^3 + \frac{16}{3\pi} \left[\frac{h}{r_f} \left(2 - \frac{h}{r_f}\right)\right]^{3/2} \tag{9}$$

So enabling the following checks: when $\frac{h}{r_f} = 0$, $M_{ep} = M_E$, at full elasticity; when $\frac{h}{r_f} = 1$, $\frac{M_P}{M_E} = \frac{16}{3\pi}$ at full plasticity giving:

$$M_P = \frac{16}{3\pi} \times \frac{\pi \sigma_y r_f^3}{4} = \frac{4\sigma_y r_f^3}{3}$$

Substituting from Eq. (6): $1 - \frac{h}{r_f} = \frac{\rho_e \sigma_y}{E_f r_f}$, the moment ratio in Eq. (9) is expressed in terms of ρ_e :

$$\frac{M_{ep}}{M_E} = \left(\frac{\rho_e \sigma_y}{E_f r_f}\right)^3 + \frac{16}{3\pi} \left[\left(1 - \frac{\rho_e \sigma_y}{E_f r_f}\right) \left(1 + \frac{\rho_e \sigma_y}{E_f r_f}\right)\right]^{3/2}$$

$$= \left(\frac{\rho_e \sigma_y}{E_f r_f}\right)^3 + \frac{16}{3\pi} \left[\left(1 - \frac{\rho_e \sigma_y}{E_f r_f}\right)^2\right]^{3/2} \tag{10}$$

in which the first elastic term may take an alternative form using I_e for the interior elastic region and I_E for the fully elastic section:

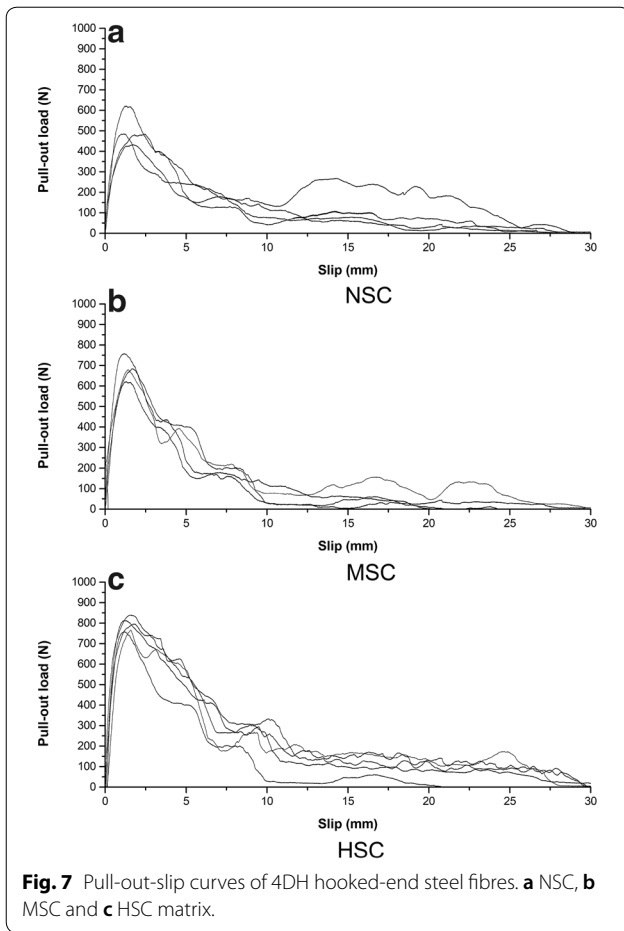


Fig. 7 Pull-out-slip curves of 4DH hooked-end steel fibres. **a** NSC, **b** MSC and **c** HSC matrix.

$$\frac{M_e}{M_E} = \frac{\sigma_y I_e}{(r_f - h)} \times \frac{r_f}{\sigma_y I_E} = \frac{I_e}{I_E} \left(\frac{r_f}{r_f - h} \right) = \frac{I_e}{I_E} \left(\frac{1}{1 - \frac{h}{r_f}} \right) \tag{11}$$

3.1 Plastic Penetration Section Geometry

The plastic zone areas $\frac{A_p}{2}$ in the Fig. 12 are in the ratio with the fibre section area A_f as:

$$\frac{A_p}{A_f} = R; \text{ where } A_f = \pi r_f^2$$

in which the geometry of Fig. 12 shows:

$$\frac{A_p}{2} = \frac{1}{2} r_f^2 (180 - 2\theta_e) \frac{\pi}{180} - r_f \cos \theta_e (r_f - h)$$

$$A_p = r_f^2 \left(1 - \frac{\theta_e}{90} \right) \pi - 2r_f^2 \left(1 - \frac{h}{r_f} \right) \cos \theta_e$$

Hence

$$\frac{A_p}{A_f} = R = \left(1 - \frac{\theta_e}{90} \right) - \frac{2}{\pi} \left(1 - \frac{h}{r_f} \right) \cos \theta_e$$

in which

$$h = r_f - r_f \sin \theta_e, \therefore \frac{h}{r_f} = 1 - \sin \theta_e; \therefore 1 - \frac{h}{r_f} = \sin \theta_e \tag{12}$$

Therefore,

$$R = \left(1 - \frac{\theta_e}{90} \right) - \frac{2}{\pi} \sin \theta_e \cos \theta_e$$

giving an equation between R and θ_e

$$\therefore R = \left(1 - \frac{\theta_e}{90} \right) - \frac{1}{\pi} \sin 2\theta_e \tag{13}$$

3.2 Curvature-Plastic Penetration Relationship

Elastic bending theory applies under the elastic contribution (M_e) to the applied moment (M_{ep}) shown in Fig. 13.

At the interface position $r_f - h$ between the two zones:

$$\frac{\sigma_y}{(r_f - h)} = \frac{M_e}{I_e} = \frac{E_f}{\rho_e} \tag{14}$$

which gives an elastic curvature ρ_e for the neutral axis (N.A) as shown:

$$\rho_e = \frac{E_f I_e}{M_e} = \frac{E_f (r_f - h)}{\sigma_y}$$

From Eq. (14)

$$\sigma_y \rho_e = E_f [r_f - r_f (1 - \sin \theta_e)]$$

$$\frac{\sigma_y \rho_e}{E_f} = r_f \sin \theta_e$$

$$\therefore \rho_e = \frac{E_f r_f \sin \theta_e}{\sigma_y} \tag{15}$$

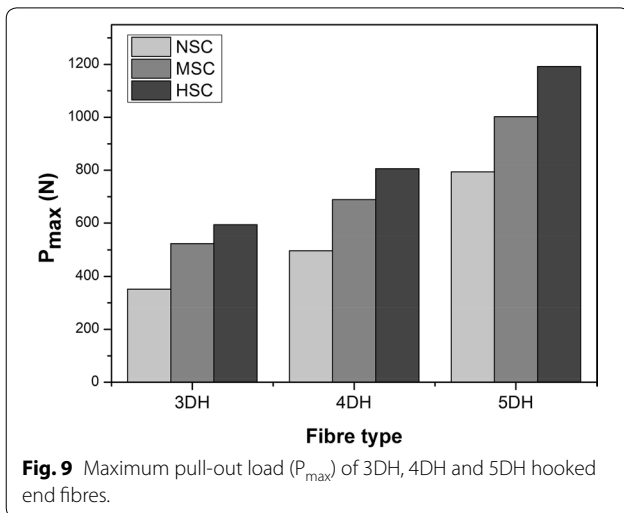
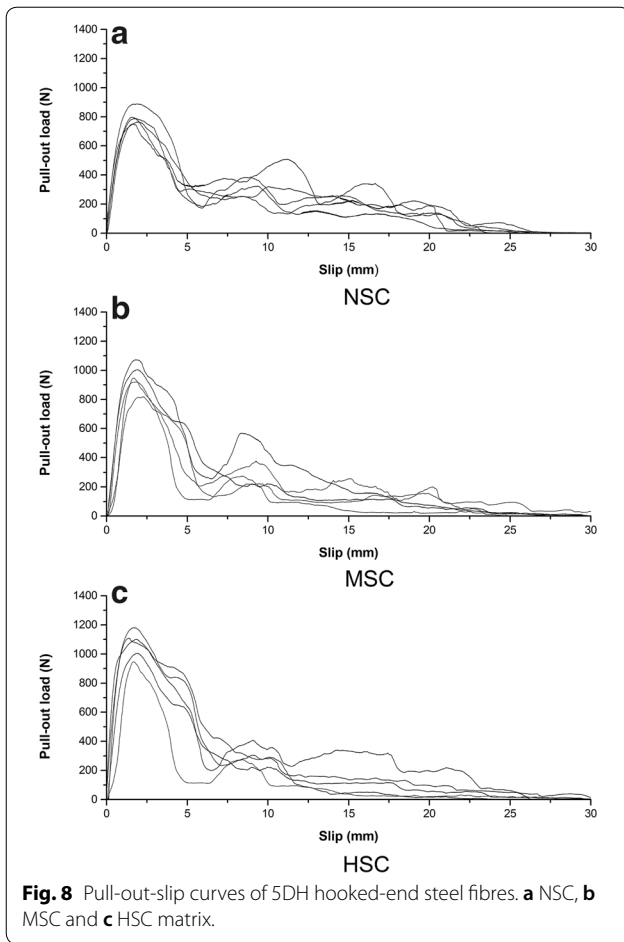
Equation (15) enables the curvature to be connected to the penetration area ratio. That is, from Eq. (13) $R = \frac{A_p}{A_f}$ is found for a given θ_e .

For example, with $R = 0.3(30\%)$ and $r_f = 0.9$ mm, $\theta_e = 35.8^\circ$ is found from Eq. (13) by trial. Then from Eq. (12) $h = 0.187$ mm when Eq. (8) gives $M_{ep} = 0.0792\sigma_y$.

The bend angle (Fig. 14) $\beta = 45^\circ$ applies to the 3DH fibre. Taking the bend length l to be a chord of a circle of curvature ρ_e shows:

$$\sin \frac{\beta}{2} = \frac{l}{2\rho_e} \tag{16}$$

Hence, for 3D fibres, where $\beta = 45^\circ$, Eqs. (10) and (11) give: $\sin \theta_e = \frac{\rho_e \sigma_y}{E_f r_f} = \frac{\sigma_y \times l}{2E_f r_f \sin(\frac{\beta}{2})} = \frac{1090 \times 2.5}{2 \times 207 \times 10^3 \times 0.45 \times \sin(\frac{45}{2})} = 0.0382$ when from Eq. (13) correspondingly,



$$\theta_e = 2.191^\circ$$

$$R = \left(1 - \frac{2.191}{90}\right) - \frac{1}{\pi} \sin 4.382 = 0.951$$

and from Eq. (12)

$$h = 0.45(1 - \sin 2.191) = 0.433$$

It appears that this initial estimate reveals too great a spread of plasticity (95.1%) when based solely upon an applied moment. Of course, when the latter is released the curvature ρ_e is altered by a partial recovery of elastic strain i.e. ‘springback’. Therefore the analysis requires an account of springback to provide the residual (initial) wire curvature ρ_R more accurately.

3.3 Account of Springback

In Fig. 15a the elastic curvature ρ_e under M_{ep} is that of the N.A within the central elastic zone. When M_{ep} is released an elastic springback occurs over the whole section for which the residual strain $\varepsilon_R = \varepsilon_e - \varepsilon_E$ connects to the required curvature ρ_R in a reciprocal relationship $\varepsilon_R = \frac{y}{\rho_R}$.

Thus at a given depth y between applying then releasing M_{ep} in Fig. 15a, b.

$$\frac{1}{\rho_R} = \frac{1}{\rho_e} - \frac{1}{\rho_E} = \frac{\rho_E - \rho_e}{\rho_E \rho_e}$$

$$\rho_R = \frac{\rho_e \rho_E}{\rho_E - \rho_e} \tag{17}$$

where the respective elastic-curvatures in Fig. 15a, b are:

$$\rho_e = \frac{E_f(r_f - h)}{Y} = \frac{E_f I_e}{M_e}$$

$$\rho_E = \frac{E_f y}{\sigma} = \frac{E_f I}{M_{ep}}$$

Substituting each elastic curvature ρ_e and ρ_E in Eq. (17):

$$\rho_R = \frac{\left(\frac{E_f I_e}{M_e}\right) \left(\frac{E_f I}{M_{ep}}\right)}{\left(\frac{E_f I}{M_{ep}} - \frac{E_f I_e}{M_e}\right)} = \frac{E_f I_e}{M_e M_{ep} \left(\frac{1}{M_{ep}} - \frac{I_e}{M_e}\right)} = \frac{E_f I_e}{I M_e - I_e M_{ep}}$$

$$\frac{\rho_R}{\rho_E} = \frac{\left(\frac{I_e}{I}\right)}{\left(\frac{M_e}{M_E} - \frac{I_e}{I} \left(\frac{M_{ep}}{M_E}\right)\right)} \tag{18}$$

Substituting Eqs. (9) and (11) in to Eq. (18)

$$\frac{\rho_R}{\rho_E} = \frac{\left(\frac{I_e}{I}\right)}{\frac{I_e}{I} \left(\frac{1}{1 - \frac{h}{r_f}}\right) - \frac{I_e}{I} \left\{ \left(1 - \frac{h}{r_f}\right)^3 + \frac{16}{3\pi} \left[\frac{h}{r_f} \left(2 - \frac{h}{r_f}\right)\right]^{3/2} \right\}}$$

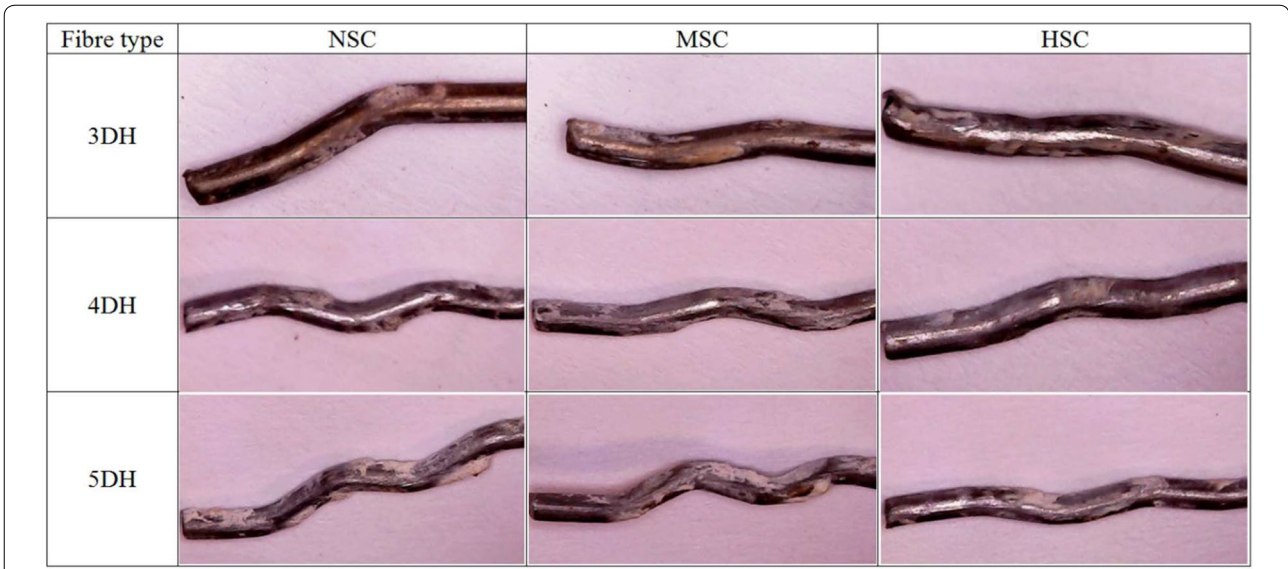


Fig. 10 Deformation and straightening of the hook after pull-out test.

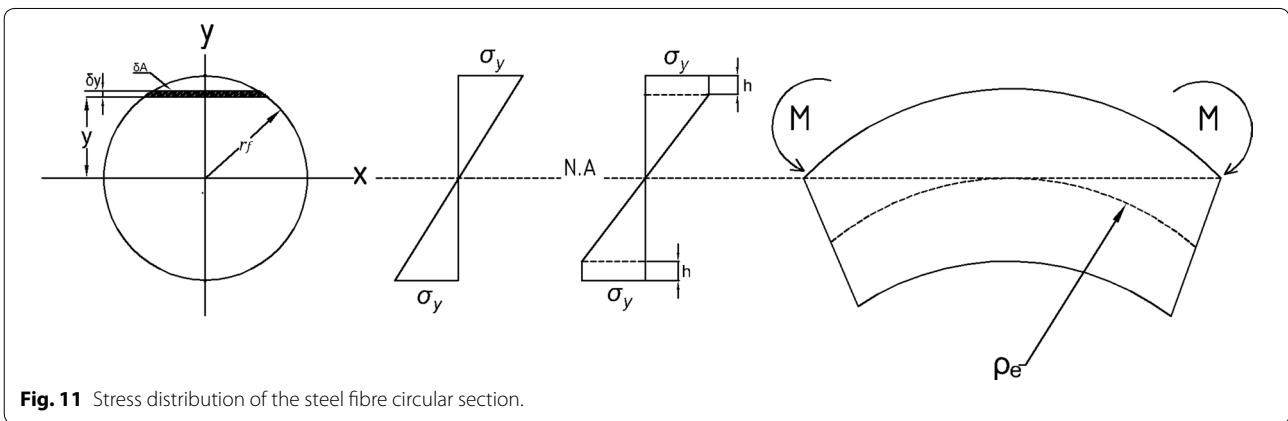


Fig. 11 Stress distribution of the steel fibre circular section.

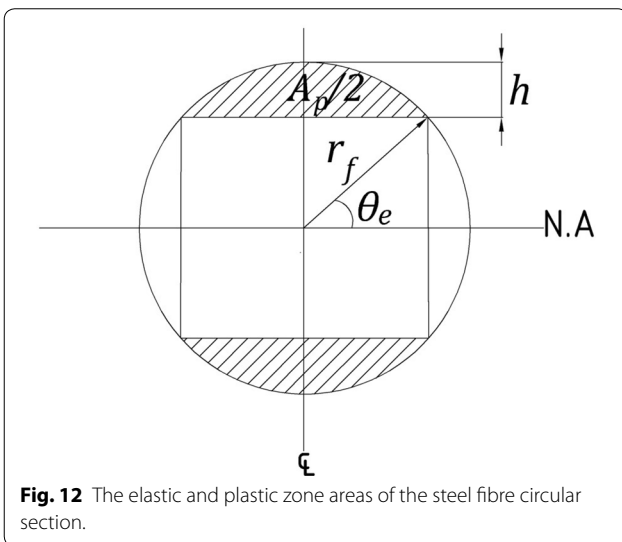


Fig. 12 The elastic and plastic zone areas of the steel fibre circular section.

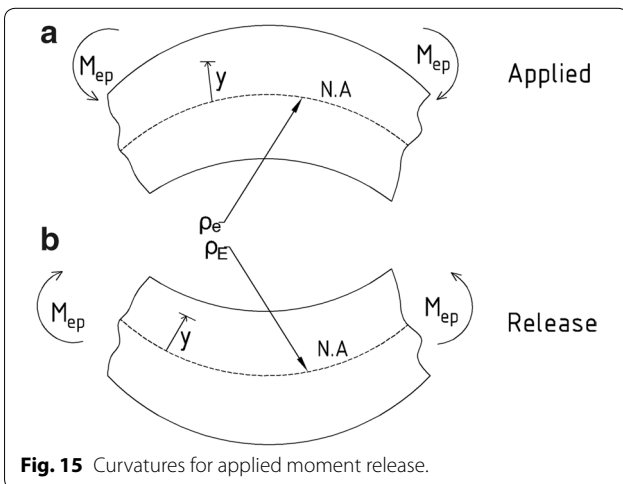
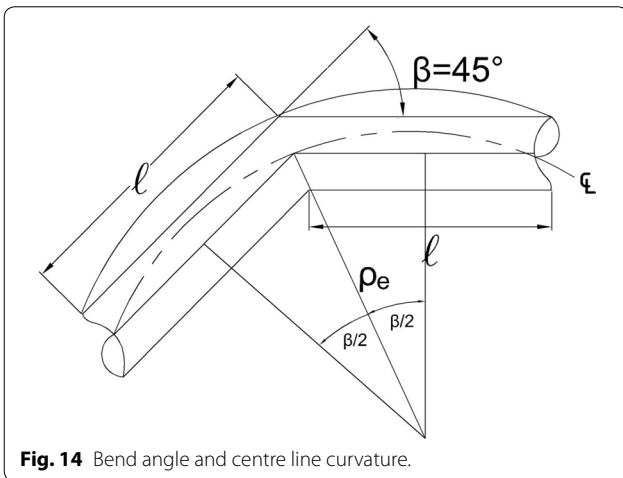
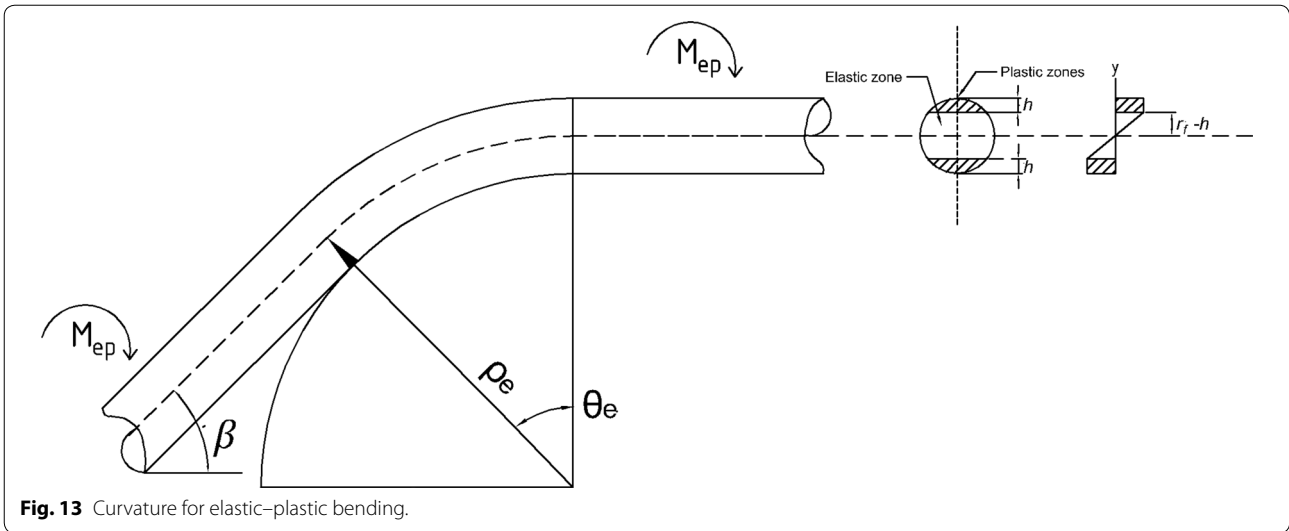
Now $I = I_E$ with an elastic recovery across the full section and therefore:

$$\frac{\rho_R}{\rho_E} = \frac{1 - \frac{h}{r_f}}{1 - \left\{ \left(1 - \frac{h}{r_f}\right)^4 + \left(1 - \frac{h}{r_f}\right) \frac{16}{3\pi} \left[\frac{h}{r_f} \left(2 - \frac{h}{r_f}\right)\right]^{3/2} \right\}} \quad (19)$$

Setting $y = \frac{\rho_R}{\rho_E}$ and $x = \frac{h}{r_f}$, Eq. (19) becomes:

$$y = \frac{1 - x}{1 - \left\{ (1 - x)^4 + \frac{16}{3\pi} (1 - x) [x(2 - x)]^{3/2} \right\}} \quad (20)$$

in which $\rho_E = \frac{E_f r_f}{\sigma_y}$ giving $y = \frac{\rho_R \sigma_y}{E_f r_f}$ for $\rho_R = \frac{l}{2 \sin\left(\frac{\beta}{2}\right)}$



The following seven-steps enable an estimate of the extent of plasticity within the equivalent bend radius of a hooked end fibre.

4 Method

1. The hook's bend angle β and straight length l approximate to an 'initial' curvature ρ_R

$$\rho_R = \frac{l}{2 \sin\left(\frac{\beta}{2}\right)}$$

2. The known yield strength σ_y , modulus E_f and fibre radius r_f provide y :

$$y = \frac{\rho_R \sigma_y}{E_f r_f}$$

3. Find x from $y = f(x)$ in Eq. (20) above
4. Find θ_e from Eq. (12): $1 - x = \sin \theta_e$

$$\theta_e = \sin^{-1}(1 - x)$$

5. Find $R = \frac{A_p}{A_t}$ from Eq. (13)

$$R = \left(1 - \frac{\theta_e}{90}\right) - \frac{1}{\pi} \sin 2\theta_e$$

6. Find h from Eq. (12)

$$h = r_f (1 - \sin \theta_e)$$

7. Find M_{ep} from Eq. (8)

$$M_{ep} = \frac{\pi \sigma_y}{4} (r_f - h)^3 + \frac{4\sigma_y}{3} [h(2r_f - h)]^{3/2}$$

Table 3 *x* and *y* values of Eq. (20).

<i>x</i>	0.1	0.2	0.3	0.4	0.5	0.6	0.7	0.8	0.9	1.0
1 − <i>x</i>	0.9	0.8	0.7	0.6	0.5	0.4	0.3	0.2	0.1	0.0
2 − <i>x</i>	1.9	1.8	1.7	1.6	1.5	1.4	1.3	1.2	1.1	1.0
Equation (16)	0.7826	0.7029	0.673	0.6509	0.6136	0.5482	0.450	0.3208	0.1673	0.0
<i>y</i>	4.14	2.693	2.14	1.719	1.294	0.8854	0.5455	0.2945	0.1201	0

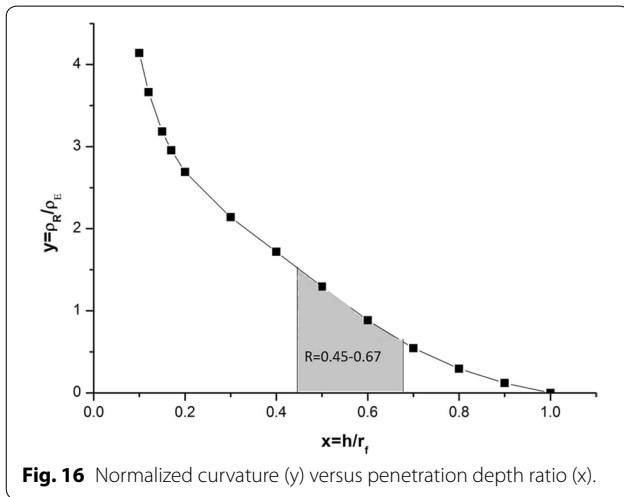


Fig. 16 Normalized curvature (*y*) versus penetration depth ratio (*x*).

Table 4 Seven-steps enable an estimate of the extent of plasticity within the equivalent bend radius of a hooked end fibre.

Method	3DH	4DH	5DH
Step 1 (ρ_R)	39.2	57.95	62
Step 2 (<i>y</i>)	0.40	0.74	0.98
Step 3 (<i>x</i>)	0.74	0.60	0.56
Step 4 (θ_e)	15.07	23.57	26.10
Step 5 (<i>R</i>)	0.67	0.50	0.45
Step 6 (<i>h</i>)	0.33	0.27	0.25
Step 7 (<i>M_{ep}</i>)	108	117	140

The graph of Table 3 entries in Fig. 16 enables *x* to be read from *y* according to step 3. All fibre geometries lie within the highlighted region shown. Thereafter the calculation of θ_e and *R* determine the spread of plasticity within the cross-section for a given fibre geometry as shown in Table 4.

5 Incorporating the Elastic–Plastic Moment Expression Into Frictional Pulley Model

The elastic–plastic moment expression proposed above (step 7) has been incorporated into frictional pulley model (Abdallah et al. 2016a) in order to predict the forces at each stage of pull-out for all hooked end fibres. From static force and moment equilibrium, the pull-out force *P* in each pull-out stage has been determined (Abdallah et al. 2016a) as given by Eqs. (21)–(24). The present mathematical interpretation of frictional pulley model has been explained in detail by Abdallah et al. (2016a).

$$\Delta P' = \frac{F_{PH}}{1 - \mu \times \cos \beta} \tag{21}$$

$$\Delta P'' = \frac{2F_{PH} \left[1 + \frac{\mu \times \cos \beta}{1 - \mu \times \cos \beta} \right]}{1 - \mu \times \cos \beta} \tag{22}$$

$$\Delta P''' = \frac{F_{PH} \left[3 + \left(\frac{2\mu \times \cos \beta}{1 - \mu \times \cos \beta} \right) \left[2 \left(1 + \frac{\mu \times \cos \beta}{1 - \mu \times \cos \beta} \right) + 1 \right] \right]}{(1 - \mu \times \cos \beta)} \tag{23}$$

$$\Delta P'''' = \frac{F_{PH} \left[4 + \left(\frac{2\mu \times \cos \beta}{1 - \mu \times \cos \beta} \right) \left[3 + 2\mu \times \cos \beta \left[2 \left(1 + \frac{\mu \times \cos \beta}{1 - \mu \times \cos \beta} \right) + 1 \right] + 2 \left(1 + \frac{\mu \times \cos \beta}{1 - \mu \times \cos \beta} \right) + 1 \right] \right]}{(1 - \mu \times \cos \beta)} \tag{24}$$

where $\Delta P'$, $\Delta P''$, $\Delta P'''$, $\Delta P''''$ represent the pull-out force due to plastic deformation contribution of one, two, three and four plastic hinges, respectively (Abdallah et al. 2016a). By adding the pull-out force at the onset of complete debonding P_1 to Eqs. (21)–(24), the pull-out force P as a function of fibre slip Δ in all main stages can be obtained as follows:

5.1 For 3DH fibre

$$P = \begin{cases} P_2 = P_1 + \Delta P'' \text{ (Eq. (18))} \\ P_3 = P_1 + \Delta P' \text{ (Eq. (17))} \end{cases} \quad (25)$$

Table 5 The predicted pull-out forces for all hooked end fibres.

Fibre type	Matrix type	P_1	P_2	P_3	P_4	P_5
3DH	NSC	55	404	264	–	–
	MSC	76	593	285	–	–
	HSC	108	625	317	–	–
4DH	NSC	55	545	454	229	–
	MSC	76	766	475	250	–
	HSC	108	798	507	282	–
5DH	NSC	55	746	834	510	255
	MSC	76	1162	855	531	276
	HSC	108	1194	887	563	308

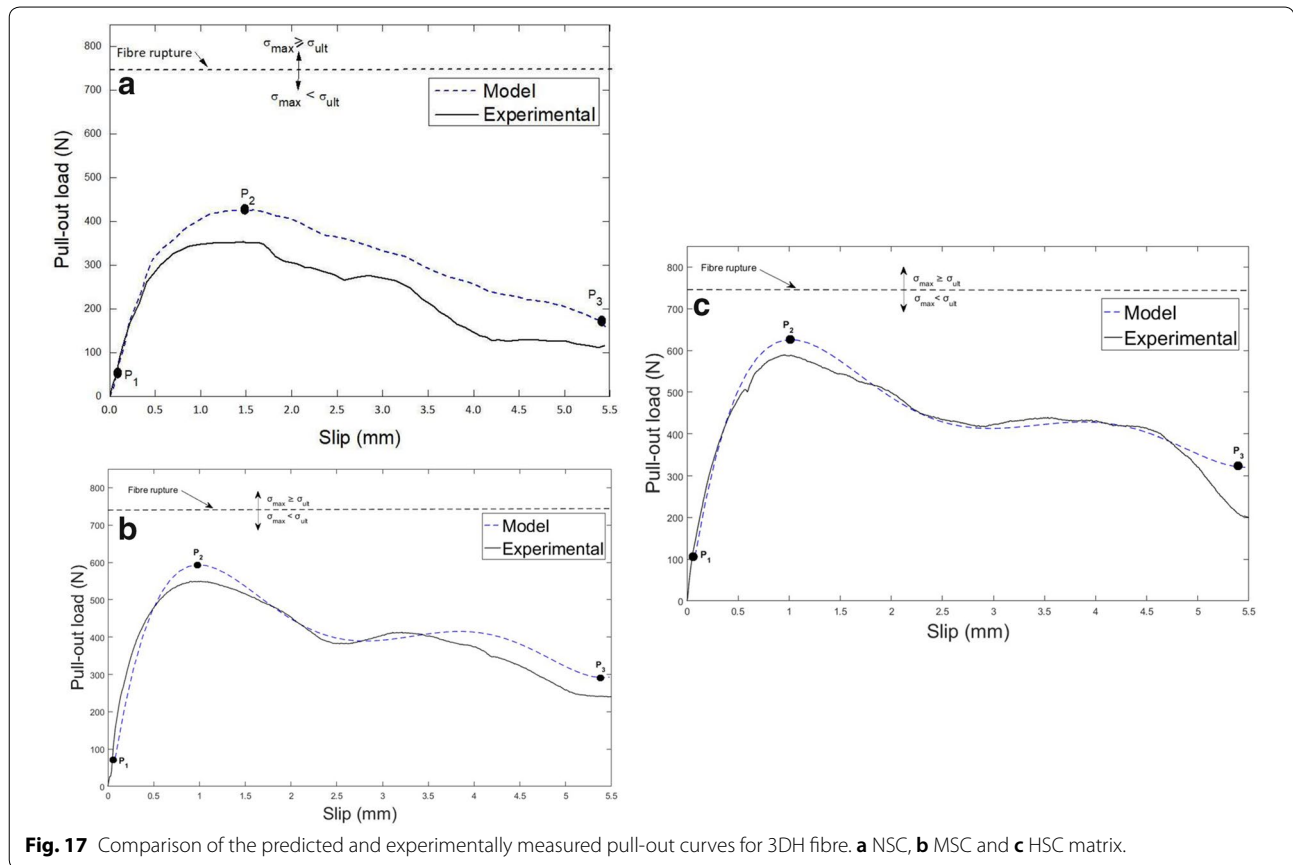
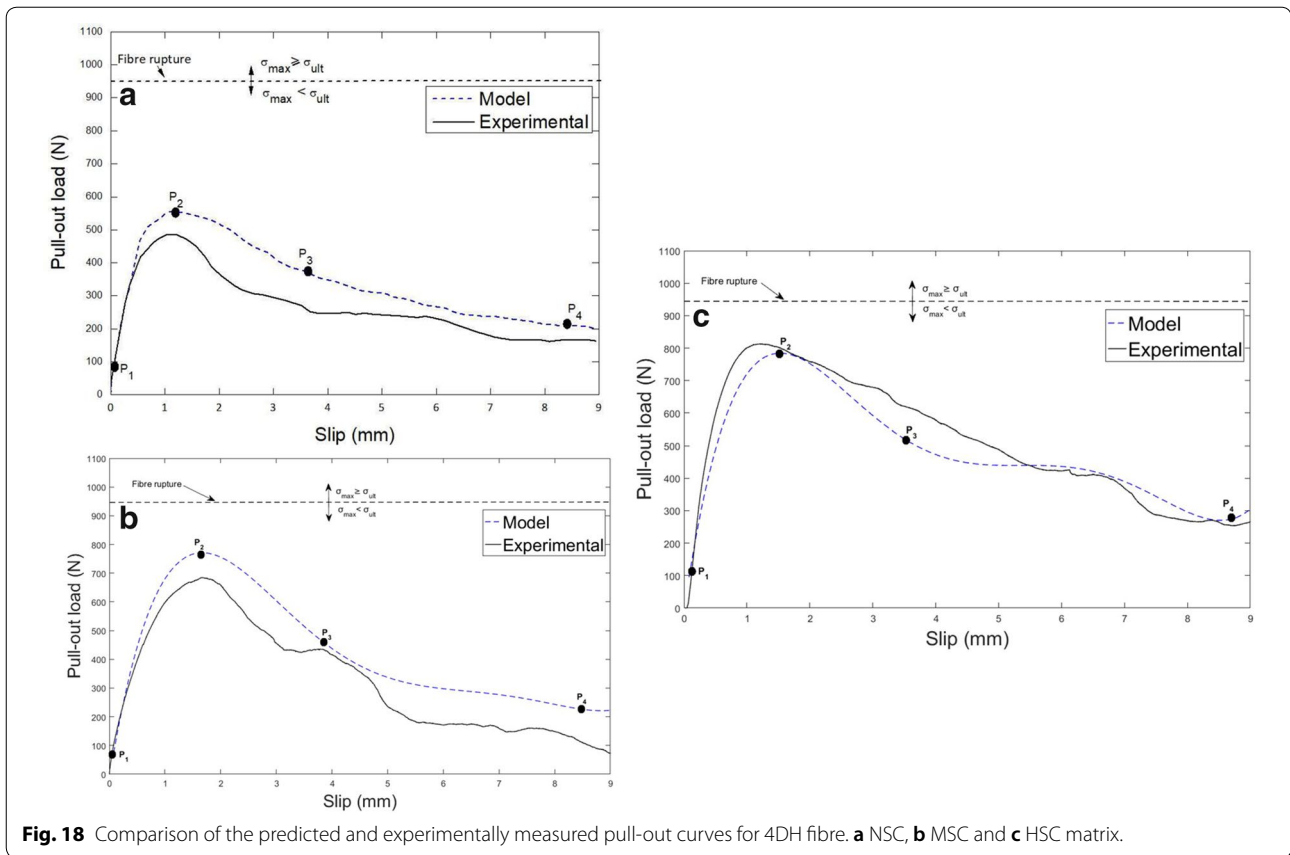


Fig. 17 Comparison of the predicted and experimentally measured pull-out curves for 3DH fibre. **a** NSC, **b** MSC and **c** HSC matrix.



5.2 For 4DH fibre

$$P = \begin{cases} P_2 = P_1 + \Delta P''' \text{ (Eq. (19))} \\ P_3 = P_1 + \Delta P'' \text{ (Eq. (18))} \\ P_4 = P_1 + \Delta P' \text{ (Eq. (17))} \end{cases} \quad (26)$$

5.3 For 5DH fibre

$$P = \begin{cases} P_2 = P_1 + \Delta P'''' \text{ (Eq. (20))} \\ P_3 = P_1 + \Delta P''' \text{ (Eq. (19))} \\ P_4 = P_1 + \Delta P'' \text{ (Eq. (18))} \\ P_5 = P_1 + \Delta P' \text{ (Eq. (17))} \end{cases} \quad (27)$$

The P_1 value can be predicted using Eq. (28) of straight fibre developed by Naaman et al. (1991a).

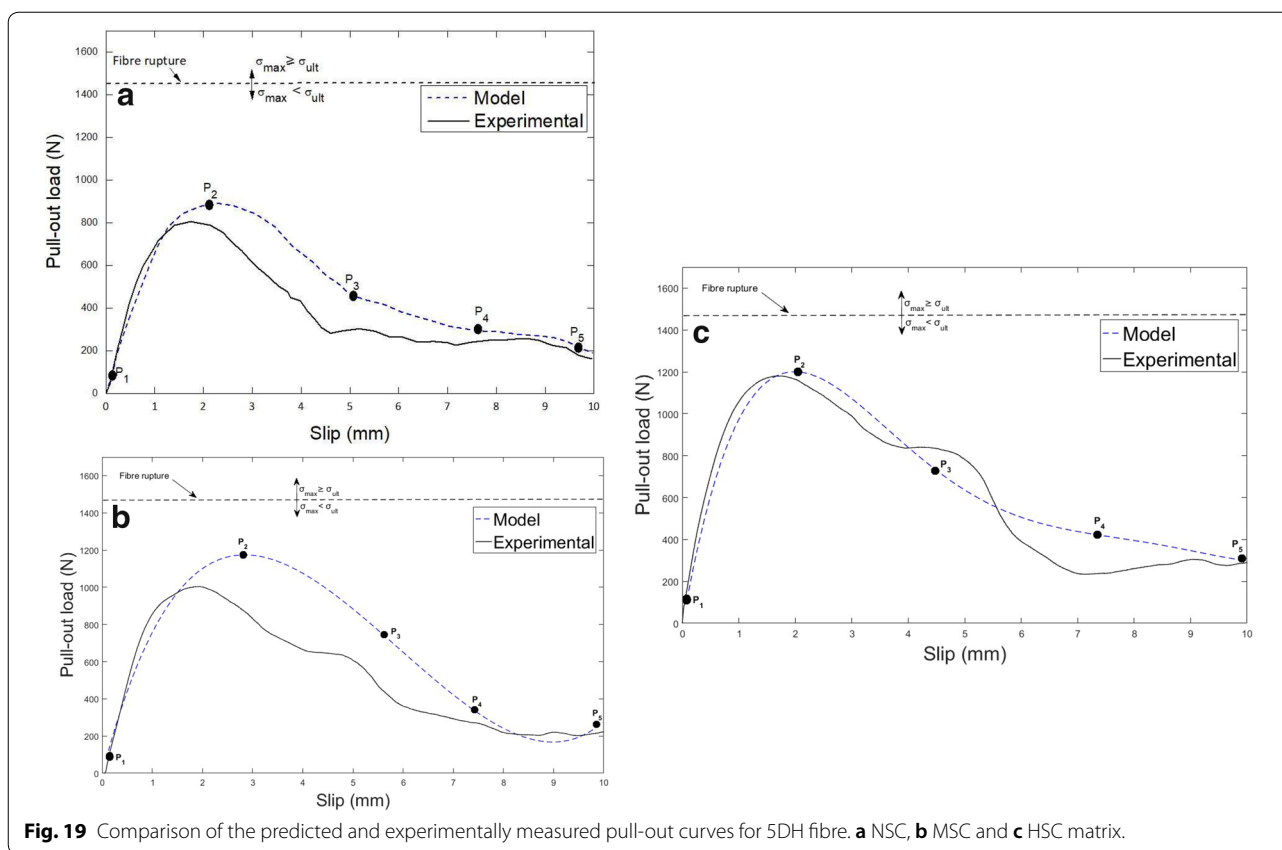
$$P_1 = \psi \tau_{fd}(\Delta) \times (l - \Delta) \quad (28)$$

where ψ is the fibre perimeter, $\tau_{fd}(\Delta)$ is the frictional shear stress function for a slip Δ , and $(l - \Delta)$ is the length of fibre remaining embedded.

6 Model Validation

The frictional pulley model predictions using the proposed elastic–plastic moment expression presented above was validated against experimental pull-out results for various hooked end fibres. All the material properties of the fibres (fibre geometry and tensile strength) as well as the concrete properties were used as the input parameters in this model (Tables 1 and 2). The predicted forces ($P_1, P_2 \dots P_5$) at each stage of pull-out for all hooked end fibres are summarized in Table 5. Here, the continuous pull-out curves shown in Figs. 17, 18 and 19 were fitted numerically to $P_1, P_2 \dots P_5$ using a fifth degree polynomial function (Abdallah et al. 2016a).

The respective figures show the comparison between the predicted and experimental pull-out curves of all hooked end fibres embedded in NSC, MSC and HSC. For each hooked end geometry, the model predictions, exhibited in Figs. 17, 18 and 19, can reasonably well simulate the experimental pull-out load-slip curve. It is clear that the proposed model is able to capture the main features of pull-out behaviour and to predict accurately the pull-out load-slip curve, irrespectively of fibre geometry and tensile strength. The model takes also into account the mechanical anchorage effect provided by the fibre



hook as well as the variation of the concrete properties. It can be observed that with increasing the matrix strength from NSC to MSC and HSC, the straightening of the hook becomes progressively increased for all fibres (Fig. 10). Therefore, the accuracy of the model predictions is increasingly improved for all fibres.

7 Conclusion

In this paper an elastic–plastic response model has been advanced to predict the pull-out behaviour of various hooked end steel fibres embedded in normal, medium and high strength concretes. The model accounts for the amount of deformation and straightening of the hook during the pull-out. The spread of plasticity within hook bends was found to be closely related to matrix strength. The elastic–plastic moment expression developed has been incorporated into frictional pulley model to predict the forces at each stage of pull-out. The input parameters to the model were the mechanical and geometrical properties of the fibres together with the ultimate strength of the concrete grades.

The proposed model has been validated against experimental results for each combination between three hooked end fibres embedded in normal, medium and high strength concretes. The results show that the

method proposed can predict the pull-out-slip response for all hooked end fibres–concrete combination realistically. Predictions show greatest accuracy in matching the pull-out-slip behaviour of hooked end fibres embedded in MSC and HSC. This model was also able to take into account matrix damage and fibre rupture.

Abbreviations

P : pull-out force; Δ : relative slip of the fibre; ΔP : pull-out force due to plastic hinges contribution; PH : plastic hinge; F_{PH} : rotational friction component; I : second moment area; M_E : elastic moment; M_{ep} : elastic–plastic moment; M_p : plastic moment; δA : incremental strip area; E_f : fibre modulus; l : the second moment of the section's area; δy : incremental strip depth; μ : friction coefficient; R : penetration depth; I_E : the second moment of the fully elastic; r_f : fibre radius; σ_y : fibre yield strength; h : plastic depth; E_f : modulus of elasticity of fibre; θ_{ϕ} : angular penetration measure; A_f : total area of the steel fibre circular section; A_p : plastic penetration area; ρ_e : fully elastic curvature; ρ_i : curvature of inner elastic zone; ρ_{ϕ} : initial curvature; ϵ_R : residual strain; ϵ_E : elastic strain.

Authors' contributions

Both authors contributed equally to this work. Both authors read and approved the final manuscript.

Acknowledgements

The first author is grateful for the financial support provided by the Ministry of Higher Education and Scientific Research of the Iraqi Government.

Competing interests

The authors declare that they have no competing interests.

Consent for publication

Authors have approved the manuscript and agree with its submission to International Journal of Concrete Structures and Materials.

Ethics approval and consent to participate

This chapter does not contain any studies with human participants performed by any of the authors.

Funding

The first author gratefully acknowledges the scholarship of the Ministry of Higher Education and Scientific Research of Iraqi Government for this Ph.D. project.

Publisher's Note

Springer Nature remains neutral with regard to jurisdictional claims in published maps and institutional affiliations.

Received: 20 May 2018 Accepted: 29 January 2019

Published online: 01 April 2019

References

- Abdallah, S., & Fan, M. (2017). Anchorage mechanisms of novel geometrical hooked-end steel fibres. *Materials and Structures*, 50(2), 139.
- Abdallah, S., Fan, M., & Cashell, K. A. (2017a). Bond-slip behaviour of steel fibres in concrete after exposure to elevated temperatures. *Construction and Building Materials*, 140, 542–551. <https://doi.org/10.1016/j.conbuildmat.2017.02.148>.
- Abdallah, S., Fan, M., & Cashell, K. A. (2017b). Pull-out behaviour of straight and hooked-end steel fibres under elevated temperatures. *Cement and Concrete Research*, 95, 132–140. <https://doi.org/10.1016/j.cemconres.2017.02.010>.
- Abdallah, S., Fan, M., & Rees, D. W. A. (2016a). Analysis and modelling of mechanical anchorage of 4D/5D hooked end steel fibres. *Materials & Design*, 112, 539–552. <https://doi.org/10.1016/j.matdes.2016.09.107>.
- Abdallah, S., Fan, M., & Rees, D. W. A. (2017c). Effect of elevated temperature on pull-out behaviour of 4DH/5DH hooked end steel fibres. *Composite Structures*, 165, 180–191. <https://doi.org/10.1016/j.compstruct.2017.01.005>.
- Abdallah, S., Fan, M., & Rees, D. W. (2018a). Bonding mechanisms and strength of steel fiber-reinforced cementitious composites: Overview. *Journal of Materials in Civil Engineering*, 30(3), 04018001.
- Abdallah, S., Fan, M., & Zhou, X. (2017d). Pull-out behaviour of hooked end steel fibres embedded in ultra-high performance mortar with various W/B ratios. *International Journal of Concrete Structures and Materials*, 11, 301–313.
- Abdallah, S., Fan, M., Zhou, X., & Geyt, S. (2016b). Anchorage effects of various steel fibre architectures for concrete reinforcement. *International Journal of Concrete Structures and Materials*, 10, 325–335.
- Abdallah, S., Rees, D. W., Ghaffar, S. H., & Fan, M. (2018b). Understanding the effects of hooked-end steel fibre geometry on the uniaxial tensile behaviour of self-compacting concrete. *Construction and Building Materials*, 178, 484–494.
- Adjrad, A., Bouafia, Y., Kachi, M., & Ghazi, F. (2016). Prediction of the Rupture of Circular Sections of Reinforced Concrete and Fiber Reinforced Concrete. *International Journal of Concrete Structures and Materials*, 10, 373–381.
- Alwan, J. M., Naaman, A. E., & Guerrero, P. (1999). Effect of mechanical clamping on the pull-out response of hooked steel fibers embedded in cementitious matrices. *Concrete Science and Engineering*, 1(1), 15–25.
- Chanvillard, G. (1999). Modeling the pullout of wire-drawn steel fibers. *Cement and Concrete Research*, 29(7), 1027–1037.
- Deng, F., Ding, X., Chi, Y., Xu, L., & Wang, L. (2018). The pull-out behavior of straight and hooked-end steel fiber from hybrid fiber reinforced cementitious composite: Experimental study and analytical modelling. *Composite Structures*, 206, 693–712.
- El-Mal, H. A., Sherbini, A., & Sallam, H. (2015). Mode II fracture toughness of hybrid FRCS. *International Journal of Concrete Structures and Materials*, 9(4), 475–486.
- Georgiadi-Stefanidi, K., Mistakidis, E., Pantousa, D., & Zygomalas, M. (2010). Numerical modelling of the pull-out of hooked steel fibres from high-strength cementitious matrix, supplemented by experimental results. *Construction and Building Materials*, 24(12), 2489–2506. <https://doi.org/10.1016/j.conbuildmat.2010.06.007>.
- Ghoddousi, P., Ahmadi, R., & Sharifi, M. (2010). Fiber pullout model for aligned hooked-end steel fiber. *Canadian Journal of Civil Engineering*, 37(9), 1179–1188.
- Isia, F., Ruano, G., & Luccioni, B. (2015). Analysis of steel fibers pull-out. Experimental study. *Construction and Building Materials*, 100, 183–193. <https://doi.org/10.1016/j.conbuildmat.2015.09.034>.
- Islam, M. S., & Alam, S. (2013). Principal component and multiple regression analysis for steel fiber reinforced concrete (SFRC) beams. *International Journal of Concrete Structures and Materials*, 7(4), 303–317.
- Laranjeira, F., Molins, C., & Aguado, A. (2010). Predicting the pullout response of inclined hooked steel fibers. *Cement and Concrete Research*, 40(10), 1471–1487. <https://doi.org/10.1016/j.cemconres.2010.05.005>.
- Lee, Y., Kang, S., & Kim, J. (2010). Pullout behavior of inclined steel fiber in an ultra-high strength cementitious matrix. *Construction and Building Materials*, 24(10), 2030–2041.
- Li, H., & Liu, G. (2016). Tensile properties of hybrid fiber-reinforced reactive powder concrete after exposure to elevated temperatures. *International Journal of Concrete Structures and Materials*, 10, 29–37.
- Naaman, A. E., Namur, G. G., Alwan, J. M., & Najm, H. S. (1991a). Fiber pullout and bond slip. I: Analytical study. *Journal of Structural Engineering*, 117(9), 2769–2790.
- Naaman, A. E., Namur, G. G., Alwan, J. M., & Najm, H. S. (1991b). Fiber pullout and bond slip. II: Experimental validation. *Journal of Structural Engineering*, 117(9), 2791–2800.
- Nammur, G. G., Jr., & Naaman, A. E. (1989). Bond stress model for fiber reinforced concrete based on bond stress-slip relationship. *ACI Materials Journal*, 86(1), 45–57.
- Robins, P., Austin, S., & Jones, P. (2002). Pull-out behaviour of hooked steel fibres. *Materials and Structures*, 35(7), 434–442.
- Soetens, T., van Gysel, A., Matthys, S., & Taerwe, L. (2013a). A semi-analytical model to predict the pull-out behaviour of inclined hooked-end steel fibres. *Construction and Building Materials*, 43, 253–265.
- Soetens, T., van Gysel, A., Matthys, S., & Taerwe, L. (2013b). A semi-analytical model to predict the pull-out behaviour of inclined hooked-end steel fibres. *Construction and Building Materials*, 43, 253–265. <https://doi.org/10.1016/j.conbuildmat.2013.01.034>.
- Sujivorakul, C., Waas, A., & Naaman, A. (2000). Pullout response of a smooth fiber with an end anchorage. *Journal of Engineering Mechanics*, 126(9), 986–993.
- Tadepalli, P. R., Mo, Y., & Hsu, T. T. (2013). Mechanical properties of steel fibre concrete. *Magazine of Concrete Research*, 65(8), 462–474.
- Tuyan, M., & Yazici, H. (2012). Pull-out behavior of single steel fiber from SIF-CON matrix. *Construction and Building Materials*, 35, 571–577. <https://doi.org/10.1016/j.conbuildmat.2012.04.110>.
- Won, J., Hong, B., Lee, S., & Choi, S. J. (2013). Bonding properties of amorphous micro-steel fibre-reinforced cementitious composites. *Composite Structures*, 102, 101–109.
- Won, J., Lee, J., & Lee, S. (2015). Predicting pull-out behaviour based on the bond mechanism of arch-type steel fibre in cementitious composite. *Composite Structures*, 134, 633–644. <https://doi.org/10.1016/j.compstruct.2015.08.127>.
- Zendaoui, A., Kadid, A., & Yahiaoui, D. (2016). Comparison of different numerical models of RC elements for predicting the seismic performance of structures. *International Journal of Concrete Structures and Materials*, 10(4), 461–478.
- Zile, E., & Zile, O. (2013). Effect of the fiber geometry on the pullout response of mechanically deformed steel fibers. *Cement and Concrete Research*, 44, 18–24. <https://doi.org/10.1016/j.cemconres.2012.10.014>.